Journal of Microscopy, Vol. 216, Pt 3 December 2004, pp. 206–214
Received 15 June 2004; accepted 31 July 2004

SHORT COMMUNICATION

Three-dimensional representation of curved nanowires

Z. HUANG, D. A. DIKIN, W. DING, Y. QIAO, X. CHEN,
Y. FRIDMAN* & R. S. RUOFF

Department of Mechanical Engineering, Northwestern University, Evanston, IL 60208, U.S.A.
**Department of Computer Science, University of North Carolina, Chapel Hill, NC 27599, U.S.A.*

Key words. Electron microscopy, epipolar geometry, nanowire, parallax method, three-dimensional representation.

Summary

Nanostructures, such as nanowires, nanotubes and nanocoils, can be described in many cases as quasi one-dimensional curved objects projecting in three-dimensional space. A parallax method to construct the correct three-dimensional geometry of such one-dimensional nanostructures is presented. A series of scanning electron microscope images was acquired at different view angles, thus providing a set of image pairs that were used to generate three-dimensional representations using a MATLAB program. An error analysis as a function of the view angle between the two images is presented and discussed. As an example application, the importance of knowing the true three-dimensional shape of boron nanowires is demonstrated; without the nanowire's correct length and diameter, mechanical resonance data cannot provide an accurate estimate of Young's modulus.

Introduction

The mechanical properties of nanostructures such as wires, tubes, coils, ribbons [for discussion purposes, we will refer only to nanowires (NWs) below], are of both fundamental and practical interest. One method of determining a NW's stiffness (Young's modulus, E) is to drive it at its mechanical resonance. This method requires that the geometry, density (mass per unit length), and resonant frequency of the NW be known. The fourth power dependence of E on the length (L) is such that an error in L of 5% yields an error in E of ~20%. The most common method of detecting mechanical resonance of NWs is to use scanning or transmission electron microscopy (SEM or TEM; Treacy *et al.*, 1996; Poncharal *et al.*, 1999; Yu *et al.*, 2002; Dikin *et al.*, 2003). It is well known that the SEM has high resolution in the plane orthogonal to the electron beam (the *XOY* plane), but low resolution in the z direction due to a large depth of focus. Determining L for a NW from one two-dimensional (2D) image only yields a good value when the NW happens to lie *exactly* in the *XOY* plane. Because this is atypical for many experiments, L would be poorly determined from a single image. This motivates developing rapid methods to determine the true dimensions and position of the NW, which will also assist in achieving rapid manipulation of the NW (and other tools in relation to it) to configure nanoscale experiments in three-dimensional (3D) space, perform rapid prototyping of devices, and ultimately carry out certain types of nanoscale manufacturing.

There is a long list of experiments performed with the aim of realizing stereo-vision by electron microscopy (Boyde, 1973; Thong & Breton, 1992; Hein *et al.*, 1999). All of these experiments involve using a series of micrographs obtained at different angles of incidence of the primary electron beam. For example, Cheng *et al.* (2000) and Hein (2001) used the parallax method to generate 3D reconstructions of cytoskeleton and to measure topography of a rough surface region, where the object's 3D coordinates are calculated from stereo pairs. The features representing each particular point are characterized by their local direction, local phase, and intensity (Cheng *et al.*, 2000). The stereo pairs are matched based on the similarity of these features to find corresponding points. To determine the 3D representation of NWs attempted here, Hein's National Institutes of Health Image Macro Tools were first used. However, the 3D reconstructions of the curved NWs were not satisfactory, which was attributed to the lack of specific landmarks on and around the NW surface to be used for effectively determining the corresponding points for Hein's program. This led to the development of another method to determine the 3D representation of one-dimensional objects, as presented here.

Methods

We chose to use epipolar geometry (Hartley & Zisserman, 2000) to match the stereo images taken by the parallax

Correspondence to: Prof. R. S. Ruoff. Tel.: +1 874 467 6596; e-mail: r-ruoff@northwestern.edu

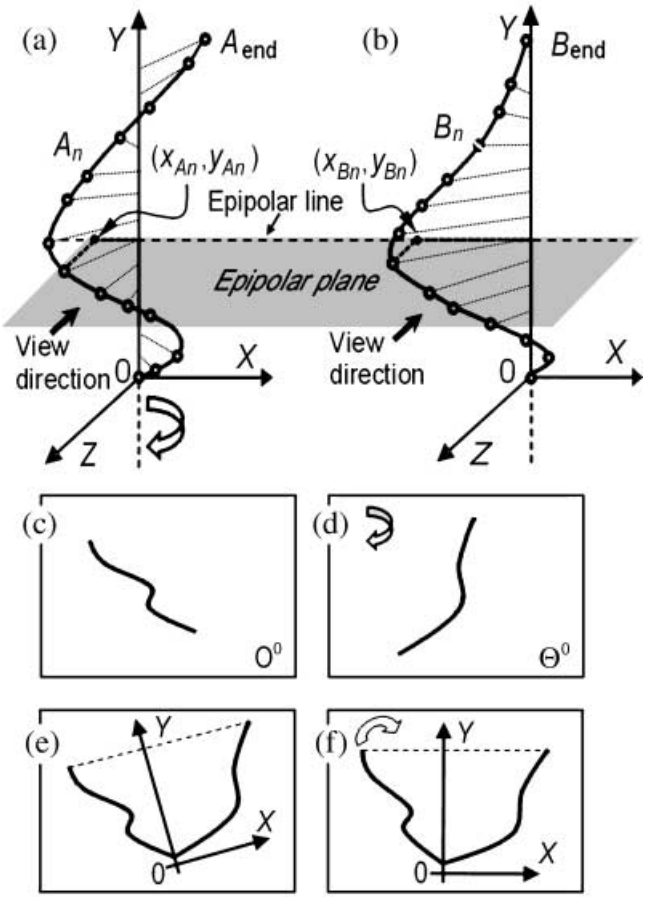

Fig. 1. Schematic representation of a wire partitioned into *N* segments (a) before and (b) after rotation. *XOY* is the image plane; the plane parallel to *XOZ* is the epipolar plane; the intersection line of the image plane and the epipolar plane is the epipolar line. (c, d) Projections of a wire onto the image plane at two different angles of rotation. (e) Overlap of the two images. The axis of rotation (*y*-axis) lies in the image plane. (f) The overlap image is rotated so that the *y*-axis is vertical.

method, and then construct the 3D model of the NWs. Henri & Peter (1996) and Bullitt *et al.* (1997) applied epipolar geometry to the 3D representation of vascular trees for surgical guidance. We will show that it also works well for curved NWs.

Electron microscope images can be regarded as the orthographic projections of an object with the size greatly magnified. The orthographic projection in electron microscopy means that the magnification for any part of the objects is constant and the perspective distortion can be neglected, which differs from the standard perspective projections in a conventional camera imaging technique. For an orthographic projection, if the view direction is along the *z*-axis and a NW is rotated around the *y*-axis, as shown in Fig. 1(a,b), then the *y* coordinate of every point along the curve does not change in the reference Cartesian coordinate system. The planes parallel to *XOZ* are called epipolar planes, and the intersection lines of epipolar planes and the image plane are called epipolar lines.

The procedure for a 3D representation of a NW from electron microscope images is as follows. First, two images of a NW (Fig. 1c,d) at different tilt/rotation angles are acquired. The upper end of the NW is identified and chosen as a 'reference' point. Another point on the NW, preferably the other end if it can be determined, is selected as the 'origin'. Two stereo images can be combined so that the 'origin' points are overlapped (Fig. 1e). If the axis of rotation (*y*-axis) is parallel to the image plane, the dashed line going through the 'reference' points of the NW (Fig. 1e) will be the same at any angle of the NW's rotation. This is the first test of the hardware configuration. If it is satisfied, then the *y*-axis is a vector going through the origin point and perpendicular to this dashed line (Fig. 1e). For processing convenience, the images will be rotated so that the rotation axis becomes vertical (Fig. 1f). The curve (representing a NW) can then be partitioned into *N* connected linear segments such that each segment has the same length in the *y* projection (Fig. 1a,b). For a precise 3D representation, we assign these linear segments to be between adjacent pixels for the initial SEM image. Each *n*-point (x_{An}, y_{An}), where *n* goes from 0 to *N* in the first image (Fig. 1a), has its corresponding point (x_{Bn}, y_{Bn}) in the second image (Fig. 1b) with the relationships: $y_{An} \equiv y_{Bn}$ and $y_{A(n+1)} - y_{An} \equiv y_{B(n+1)} - y_{Bn}$. Assume we draw a line normal to the *y*-axis from each point on the curve (A_n) as it resides in the 3D space. From the series of SEM images, we can record the different projection lengths of these normal lines along the *x* direction (x_{An}, x_{Bn}, as shown in Fig. 1a,b) when the curve is rotated around the *y*-axis. Based on these *x* coordinate pairs and the known angle of rotation, θ, the *z* coordinate of each point along the curve is

$$z_n = \frac{x_{An}\cos\theta - x_{Bn}}{\sin\theta} \qquad (1)$$

A series of SEM images were taken using a LEO 1525 FEG-SEM. The sample rotation can be achieved by tilting the SEM specimen stage or by using the rotation/tilt motion capabilities of our home-made nanomanipulator (Dikin *et al.*, unpublished data) attached to the SEM specimen stage. In both cases, the rotation axis (*y*-axis) is designed to be perpendicular to the view direction and parallel to the image plane.

The specimen stage in the SEM has a range of tilt angles from 0 to 90°. According to the LEO SEM specification, the tilt specimen stage has a constant error for all angles of ±0.1°. If our nanomanipulator is attached to the tilt specimen stage, its size does not allow the stage to tilt more than 20°. The nanomanipulator platform has a rotation/tilt stage (Θ-stage) with an unlimited range of tilt angles, which is used to rotate a NW with respect to the imaging direction. The motion of the Θ-stage is controlled by an 8763 iPico Driver Kit (New Focus Inc., San José, CA). The calibration procedure of the stage will be discussed later. Unfortunately, eucentric tilting is unattainable with our samples due to misalignment between the NW's position and the axis of rotation. So, when the NW holder is tilted even a relatively small amount, the NW moves laterally and

out of the field of view. Thus, the NW must be re-positioned in the field of view by x or y motors after each rotation.

As an example of this procedure, the projection of a carbonized polyacrylonitrile nanofibre attached to an AFM cantilever tip (NSC12, MikroMasch, Portland, OR) was analysed. The carbonized polyacrylonitrile nanofibres were created by electrospinning (Theron *et al.*, 2001) followed by a series of high-temperature treatments. The cantilever was placed on the Θ-stage of our nanomanipulator and put into the SEM chamber. The initial position of the NW was assigned to be at 0° tilt, and other projection images were acquired at different view angles (maximum 30°) relative to the initial position.

Figure 2(a) and (b) are SEM images of the polyacrylonitrile nanofibre at $\theta = 0$ and 30°, respectively. Figure 3(a–c) shows three 3D representations based on the image pairs at $\theta = 0$ and 5°, 0 and 15°, and 0 and 30°, respectively. The procedure to create these 3D representations is as follows. First, the NW is digitized using the TUBE TRACER program written in MATLAB (Fridman *et al.*, 2003). The TUBE TRACER program tracks the medial axis of the NW so that it may be represented as a one-dimensional curve. Although this tracing procedure has sub-pixel accuracy, the y coordinate data points were rounded to single pixel accuracy so that the corresponding points could be conveniently matched. The time required for tracing is only dependent on the NW's length and width in pixels. The NW with an area of ~2500 pixels in Fig. 2(a) was processed in 30 min on a Pentium4 2.8 GHz desktop. The 3D representation found in Fig. 3(c) provides the NW's length: 33.3 ± 0.6 μm.

To speed up this process, we also developed the 'manual tracking' function in our program that allows the operator to partition the curve manually into a certain number of segments. An operator selects several points (including two ends) along the NW in the first image. After one end of the NW in the second image is chosen, the epipolar lines will show up automatically. The cross points of the epipolar lines and the NW are the suggested corresponding points. An operator may follow this suggestion or come back and choose other points of interest. Then, the simplified 3D model will be constructed based on the calculated z coordinates of these chosen points, as for example shown in Fig. 4. This is sufficient for robotic applications, which will be discussed further in the Applications section.

The main limitation of this 3D representation method is that any segments of the NW that are lying in the epipolar plane cannot be correctly constructed (Henri & Peter, 1996, Bullitt *et al.*, 1997). The circled portion in Fig. 2(a,b) demonstrates a segment of the NW that lies very close to the epipolar plane. No matter what the real shape of the segment that lies in the epipolar plane is, the segment's projection in the image plane will always be a straight line. Figure 5 shows how this segment is improperly represented due to this limitation. This is a major issue in the detailed representation of complicated structures. However, one can obtain the correct 3D representation of most NWs if they are properly configured. For

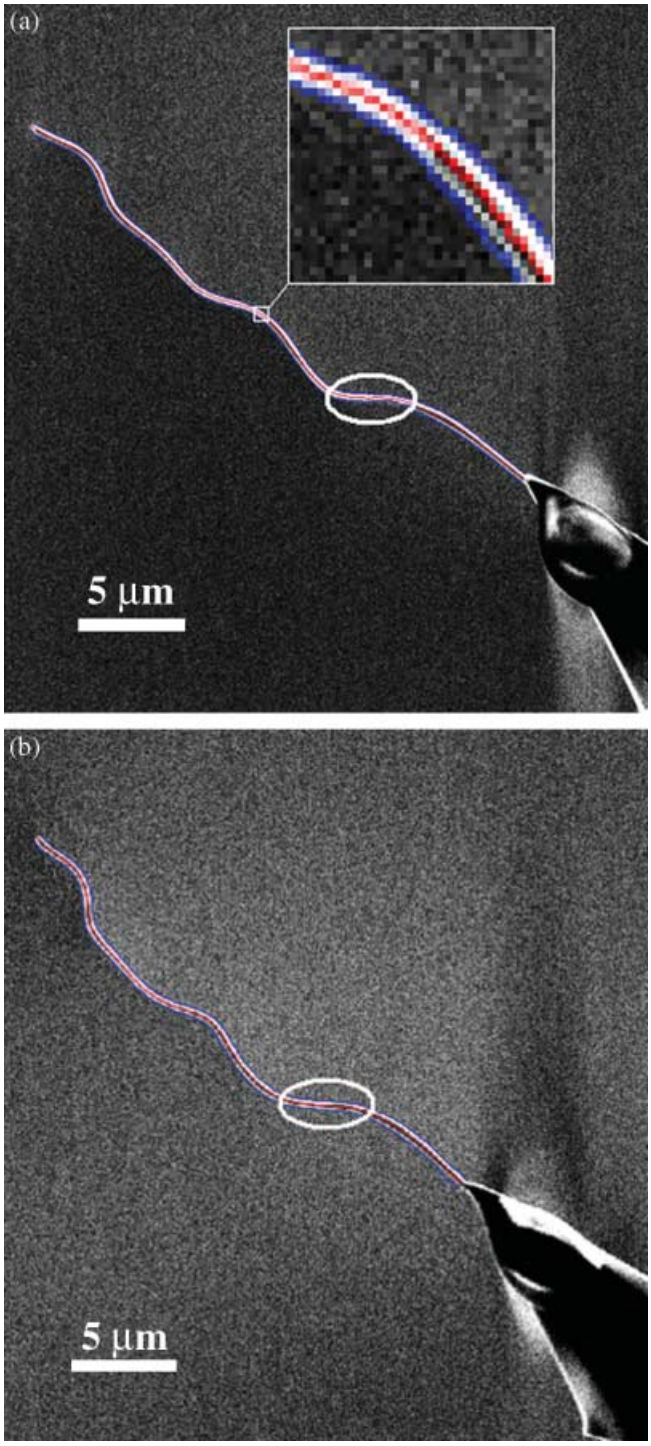

Fig. 2. Scanning electron microscope (SEM) images of the nanowire (NW) attached to an AFM tip and viewed at two angles: (a) $\theta = 0°$, (b) $\theta = 30°$. The red curve is the medial axis of the NW and the two blue curves are its boundaries computed using tube tracing (see also insert of (a)). The circled segment is discussed further in the text and in Fig. 5.

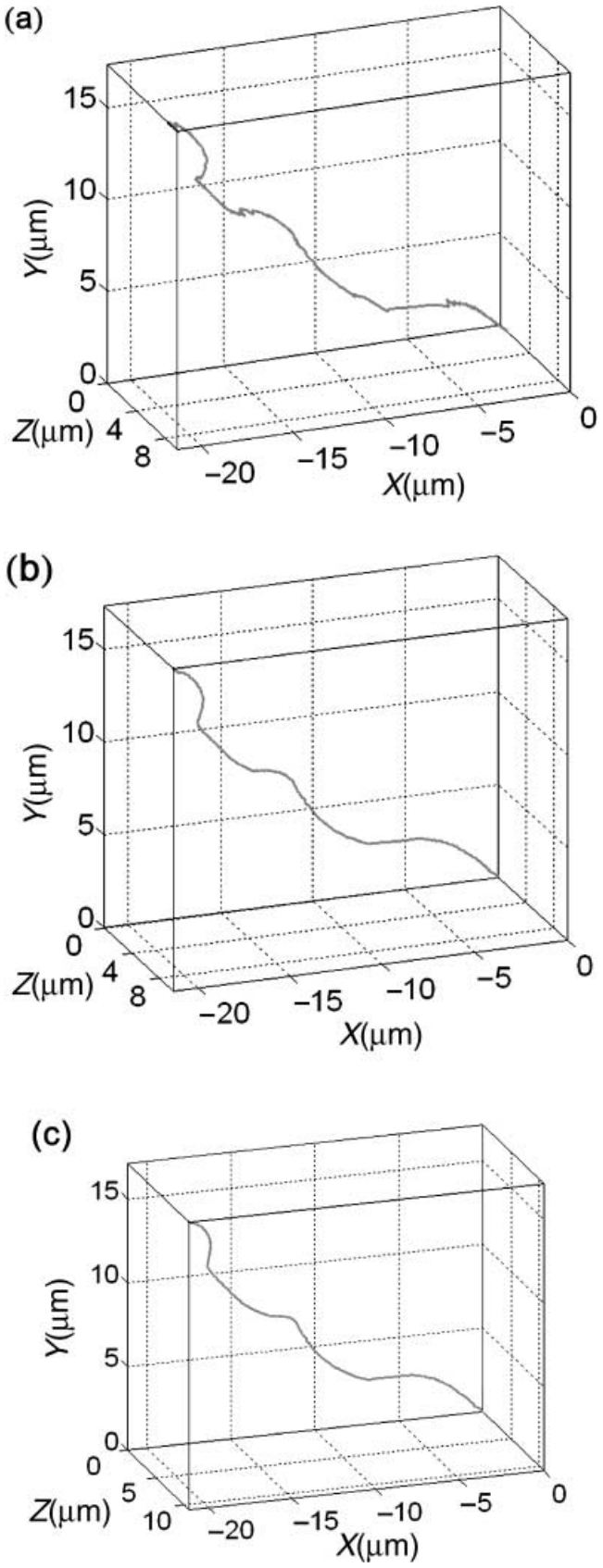

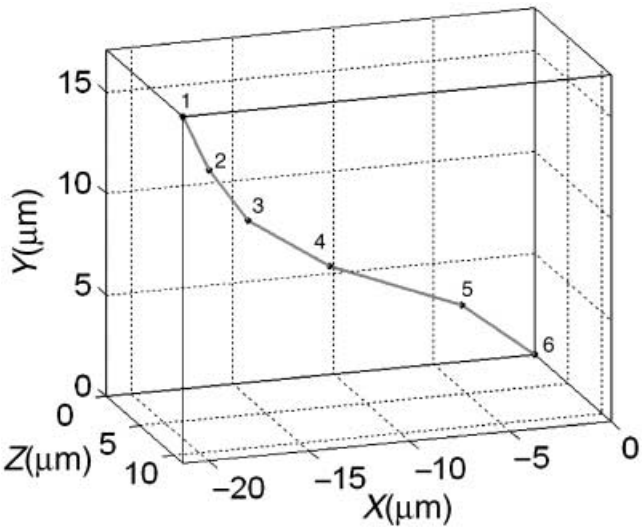

Fig. 4. A three-dimensional (3D) representation of the nanowire (NW) based on six manually chosen points and determined from the stereo image pair taken at θ = 0 and 30°.

example, if the NW in Fig. 2 can be rotated around the *z*-axis through a small angle, the segment previously lying in the epipolar plane can be properly represented. Ideally, one would have this degree of freedom available; if not, an obvious assumption is to approximate this segment by a straight line connecting the correctly constructed portions of the NW. This approximation was used to construct the short segment of NW circled in Fig. 2(a,b). A more complicated NW geometry may encumber or slow down an effective way to determine some corresponding points along the wire based on epipolar geometry. Fortunately, many NWs have straight or slightly curved shapes such as the one portrayed in this paper.

In the MATLAB program developed here, *L* can be estimated by integrating the total number of pixels (actually, voxels; the pixel size is the same along the *x*, *y*, and *z* coordinates) of the 3D curve and dividing by the total magnification. However, this approach is not accurate due to small variations that arise from a finite pixed size. The diameter of the NW in Fig. 2 is five to six pixels wide in the image. The solid folded line, shown in Fig. 6, is the medial axis of the NW traced using the TUBE TRACER program. The length of the centreline is well fitted using a line segment (dashed line in Fig. 6) over a short section, whereas the total length of the folded line will be longer than the real length of the NW, if the NW is smooth and does not have many kinks. The approximation used is to 'bin' the pixels. The length is calculated using the number of pixels similar

Fig. 3. Three-dimensional (3D) representations of the nanowire (NW) based on the two view angles. The first angle is always the same, 0°. The second angle is 5° in (a), 15° in (b), and 30° in (c). $L = 33.3$ μm and the endpoint has coordinates ($x = -21.1$ μm, $y = 17.1$ μm, $z = 11.0$ μm) as determined from the 3D representation based on images acquired at 0 and 30°.

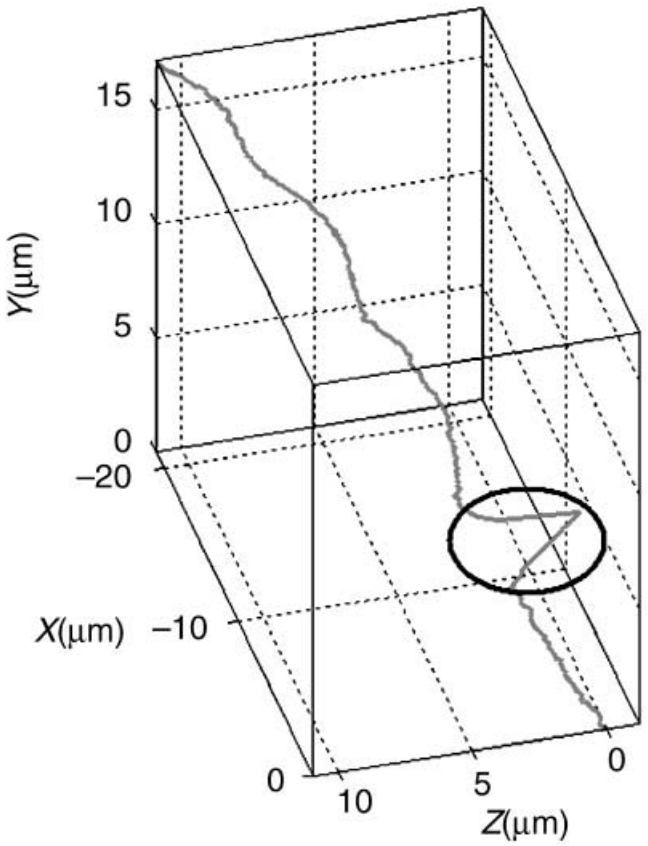

Fig. 5. The three-dimensional (3D) representation of the nanowire (NW) shown in Fig. 2. Note that the segment circled in Fig. 2 was in the epipolar plane and thus cannot be properly represented.

to the diameter of the NW rather than one pixel as the step size. For the NW in Fig. 2, the step sizes of three to six pixels were tried until the difference in integrated length based on two adjacent step sizes was smaller than 1%.

Error analysis

Before SEM images of the NW were taken, the 8763 iPico Driver in conjunction with the Θ-stage was calibrated. A sequence of electrical pulses was sent to the Θ-stage and by tracking the size change of the calibrated pattern attached to the stage, the angle of rotation was determined. This procedure does not require one to know the absolute size of the calibrant. The imaged features can be microscopically large. We drove the Θ-stage clockwise and anticlockwise up to 60° of rotation several times. The average step size was found to be 42.8 ± 0.4 mdeg or 0.747 ± 0.007 mrad.

From the 3D representations in Fig. 3(a–c), it is clear that the 3D representation based on the image pair acquired at 0 and 5° has unreal 'spikes', whereas those based on $\theta = 0$ and 15° or 0 and 30° are smoother. To analyse the validity of the 3D representation, five equally spaced points along the *y*-component of the NW (with point 1 at the top and point 5 at the bottom)

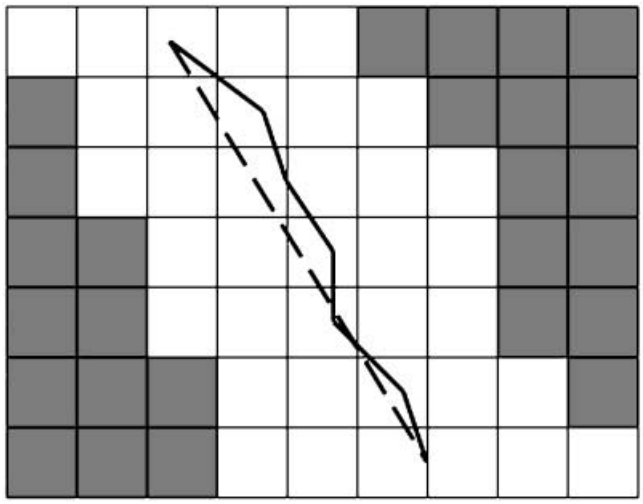

Fig. 6. Schematic (pixelated) representation of the nanowire (NW) fragment. Bright pixels represent the NW, and dark pixels are the background. Binning of pixels results in a representation (dashed line) that can be compared with the medial axis representation (solid curve) based on the use of all the bright pixels.

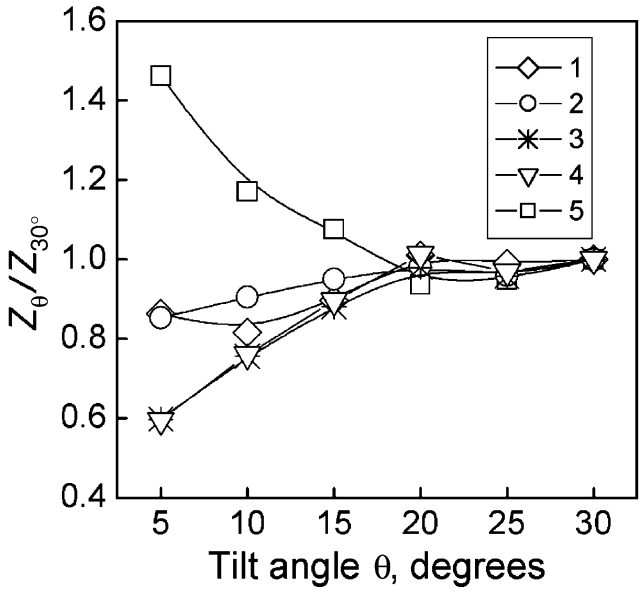

Fig. 7. The *z* coordinates of five points along the nanowire (NW) of Fig. 2, normalized to their values at view angle $\theta = 30°$, and plotted as a function of view angle. The first image z coordinate was based on assigning $\theta = 0°$; thus each Z_θ value is determined by the six image pairs at, in degrees, (0,5) (0,10) (0,15) (0,20) (0,25), and (0,30). The original NW is shown in Fig. 2 and the five analysed points (1–5) are shown in Fig. 4.

were chosen to compare their *z* coordinates. Figure 7 depicts the normalized *z* coordinates of the selected five points using the image at $\theta = 0°$ and each of the other six tilt angles (5, 10, 15, 20, 25, 30°). For $\theta > 15°$, the *z* coordinate stabilizes for all five points, indicating a decrease in the uncertainty of the z

coordinate values. Larger tilt angles improve the accuracy of the representation.

Equation (1) indicates that the absolute error, Δz_n, of the calculated value of the z coordinate is caused by the error in the rotated angle, $\Delta\theta$, and errors in the projection length, Δx_{An} and Δx_{Bn}. The projection lengths, x_{An} and x_{Bn}, are defined by $x_{An} = x_{An0}/M$ and $x_{Bn} = x_{Bn0}/M$, where x_{An0} and x_{Bn0} are the projection lengths seen on the SEM output device and M is the magnification of the SEM. Note that we can assume x_{An0} and x_{Bn0} have no error. However, the magnification (or scaling factor) does have error associated with it, so only this magnification error leads to the errors Δx_{An} and Δx_{Bn}. The error in the z coordinate (Δz_n) due to $\Delta\theta$ and ΔM is

$$\Delta z_n = \left| \frac{x_{An0} - x_{Bn0}\cos\theta}{M\sin^2\theta} \right| \Delta\theta + \left| \frac{x_{Bn0} - x_{An0}\cos\theta}{M^2\sin\theta} \right| \Delta M. \quad (2)$$

The LEO specimen stage has a constant absolute error in tilt angle ($\Delta\theta$) that is independent of the tilted angle value. The magnification error can be minimized by adjustments to the aperture, beam astigmatism, and focus. Equation (2) indicates that as θ increases, the absolute error tends to decrease because of the $\sin^2\theta$ and $\sin\theta$ terms in the denominator. However, due to the impact of $x_{An0} - x_{Bn0}\cos\theta$ and $x_{Bn0} - x_{An0}\cos\theta$, the absolute error can become larger or smaller for certain combinations of angles, and x_{An0} and x_{Bn0} values. Except for these particular cases, the 3D representation is in general better for a larger tilt angle difference in the image pair. The absolute error $\Delta\theta$ of our nanomanipulator's Θ-stage increases linearly with the rotation/tilt angle. However, the relative error analysis shows the same trend as the LEO specimen stage: a large difference in tilt angles decreases the representation error.

Equation (2) has a very simplified form, and does not include the mismatch angle between the axis of rotation and the image plane, all possible registration errors, and the aberrations in the microscope optics. It also does not include the error associated with manual selection of points along the wire.

A perfectly aligned axis of rotation (tilt axis) within the image plane is the most critical requirement for using the rules of epipolar geometry. A small tilt angle will minimize the error due to the mismatch between the axis of rotation and the image plane. However, increasing the angle of the object rotation results in decreasing the errors of the NW coordinates, as shown above. That is why we did not tilt the NW much more than 30°, which is a good compromise angle for the 3D representation.

The aberration in the microscope optics from the circular symmetry, which is called astigmatism, will result in unidirectional image defocusing. It certainly will be a cause of error in the determining the correct wire coordinates. This should be avoided by careful microscope adjustments, especially when operating at high magnification (above ~50 kX).

For the manual selection of points, the operator should select the centre point of the wire as accurately as possible – ideally as accurately as it is performed by the computer. However, this will not typically be possible because the computer tracing achieves subpixel fitting. The manually selected errors for Δx_{An} and Δx_{Bn} are essentially the same, about one pixel in our cases, when the NW diameter is five to 10 pixels across. For example, in the zoomed-in image of Fig. 2 the NW diameter is about 300 nm and the pixel size is 58.6 nm. The absolute error of the calculated z as the function of the errors associated with an operator picking the 'centre point' manually is:

$$\Delta z = |\Delta x_{An} \cdot \tan^{-1}\theta| + |\Delta x_{Bn} \cdot \sin^{-1}\theta| \quad (3)$$

This error decreases as the tilt angle becomes large. At 5° between the initial and tilted positions Δz is 1.34 μm, at 10° is 669 nm, at 20° is 332 nm, at 30° is 218 nm, and at 40° is 161 nm. It is important that at the tilt angle of 30° the error in the z direction becomes smaller than the wire diameter, which is already good enough for most goals of manipulation.

An SEM calibration grid (grid size 463 nm, SIRA Calibration Specimen, Ted Pella Inc., Redding, CA) was used to test the accuracy of obtaining L. The calibration grid was placed directly on the LEO SEM tilt specimen stage. The stage was tilted to different angles and images obtained. Figure 8(a) and (b) show images collected with the tilt angles $\theta = 0$ and 30°. The tilt angle of 30° with respect to the electron beam was used to approximate the typical experimental situation in which a nanostructure projects out into space and is not simply lying in the *XOY* plane. This position was assigned 'tilt angle = 0°'. Figure 8(c) shows a zoomed-in image of the grid, which allowed us to pick a particular pixel to use in the image. This option is very helpful in correctly selecting special points along the NW assigned for representation. Figure 8(d) shows the 3D representation of a line segment that has a length of 10 grid units. The measured L is 4.72 μm; thus, the average length of each grid unit is 472 nm, giving a relative error of 1.9% when compared with the nominal grid size (463 nm). This is a high-quality quantitative result considering that the total measured error is a sum of the SEM grid manufacturer spacing error (1%), the SEM translation specimen stage tilting accuracy (±0.1°), the uncertainty in the identification of the corresponding points, the error of the SEM magnification (<5%), and image distortions.

This SEM grid was also used to calibrate the rotation/tilt accuracy of the Θ-stage of our home-built nanomanipulator.

Applications

As previously mentioned, the true length L of a NW is a critical parameter in fitting Young's modulus, E, to mechanical resonance data, as E is proportional to the fourth power of L. The measured length of a NW obtained from one SEM image (we call this the '2D length') is reliable only when the whole NW lies in the image plane. So, the orientation of the NW needs to be carefully adjusted to guarantee that it is the largest length

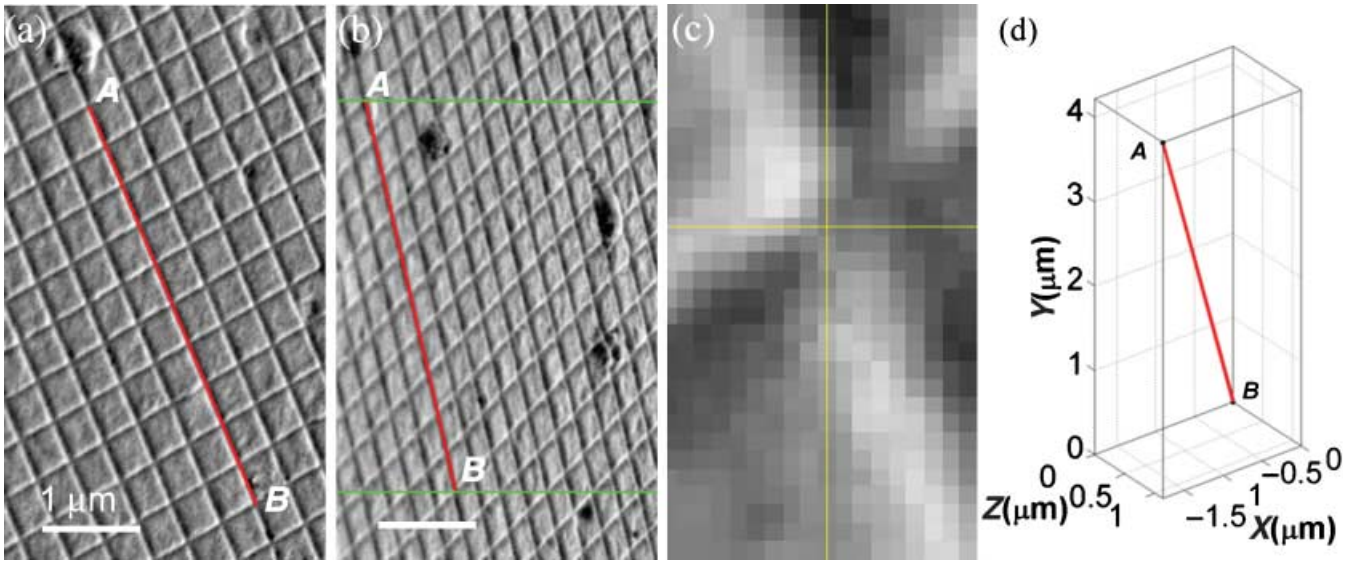

Fig. 8. Scanning electron microscope (SEM) image of the SIRA calibration specimen at two view angles: (a) θ = 0°, (b) θ = 30°. (c) The zoomed-in image used to choose one pixel (point *A*) for each of the stereo image pairs. (d) The end point *A* has coordinates: $x = -1.78$ μm, $y = 4.22$ μm, $z = 1.14$ μm with point B at the origin; thus, $L = 4.72$ μm.

Table 1. Young's modulus error due to not having a three-dimensional representation of the boron nanowires.

Sample number	Two-dimensional length (L_{2D}; μm)	Three-dimensional length (L_{3D}; μm)	Length error (%)[a]	Error in Young's modulus (%)[b]
A	11.9	13.7	13.1	43.1
B	17.0	17.8	4.5	16.8
C	5.46	6.05	9.8	33.7
D	16.4	19.3	15.0	47.9
E	5.49	6.50	15.5	49.1

[a] $|L_{3D} - L_{2D}|/L_{3D} \times 100\%$.
[b] $|E_{3D} - E_{2D}|/E_{3D} \times 100\%$.

in the *XOY* plane. To do this, the 2D length of the NW has to be measured precisely after each adjustment, a very time-consuming process. However, even this does not guarantee that the 2D imaged length is the full NW length. Only the process of acquiring at least two images taken at different view angles can provide information about the true NW length. (We call this the '3D length', obtained from the 3D representation.)

Table 1 shows measured 2D and 3D lengths of boron NWs, and also the error in Young's modulus calculated based on the resonance vibration of these wires. For a singly clamped uniform beam, the mechanical resonance frequency f_n for the nth mode is (Timoshenko, 1936; Bishop & Johnson, 1960)

$$f_n = \frac{\beta_n^2}{2\pi}\sqrt{\frac{EI}{A\rho L^4}}. \qquad (4)$$

Here β_n is the eigenvalue obtained from the characteristic equation $\cos h(\beta_n)\cos(\beta_n) = -1$, I is the wire momentum of inertia, A is the wire cross-section, and ρ is the material density. Note that in Table 1, L_{2D} is the longest 2D length found from a series of images taken in the SEM and L_{3D} is the length of the NW obtained by 3D representation. It is remarkable that although all boron NWs appear to lie in the image plane (Fig. 9), actually they do not. For relatively small errors in length ($\Delta L/L$), the error in the modulus, $\Delta E/E$, is ~4($\Delta L/L$). As a result, the error in Young's modulus approaches 50%, simply due to the uncertainty in NW length determination. Of course, other variables in Eq. (4), such as the uniformity along its length, its density, and the boundary conditions, are also critical, as discussed by Chen *et al.* (2004).

The rapid 3D representation of any objects inside the SEM will also find application in robotic nanomanipulation. The 3D representation provides information about the positions of a NW (a full set of x, y, z Cartesian coordinates of the NW, which can be transformed to any angle of rotation) and other nanotools in 3D space, so that the manipulator can approach and interact with the NW in a controlled manner. Speed is

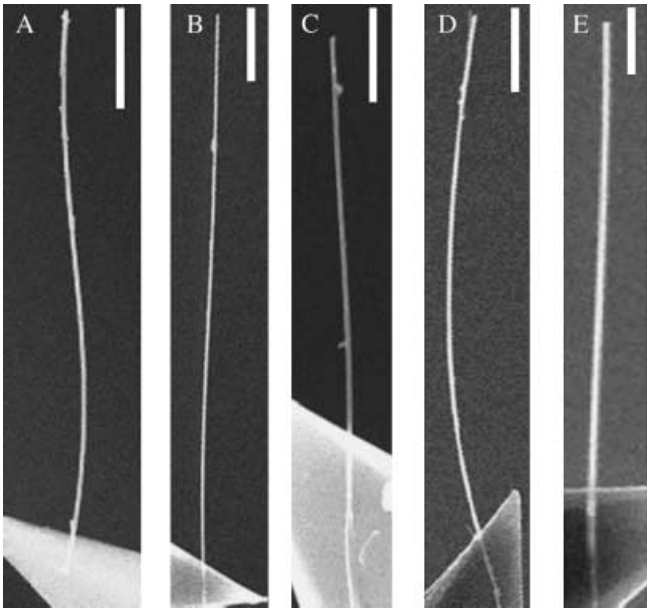

Fig. 9. Scanning electron microscope (SEM) images of the five boron nanowires (NWs) cited in Table 1. The scale bar for samples A, B, D, and E is 2 μm, and for sample C is 1 μm.

essential for robotic manipulation, so using the tube tracing method described above and having a tracing time of the order of 30 min is impractical.

A time-saving function in our program is manual tracking. This function was developed to obtain the 3D coordinates of particular points along the NW in real time and to generate a simplified 3D representation. By using the manual tracking function, an operator can pick several points (pixels) along the NW image, and computer-processing time for the simplified 3D representation of the NW will be almost negligible. So, the 3D representation will include a set of coordinates of the NW special points, which can then be traced to any new NW position and compared with coordinates of other nanomanipulator tools. These coordinates are critical in the positioning of different nanomanipulator components, e.g. nanoelectrodes or nanotweezers, with respect to the NW for nanorobotic manipulation and other nanoscale experiments.

Conclusions

Epipolar geometry was used to find corresponding points and to construct the 3D representation of NWs with stereo image pairs obtained in a SEM, based on the parallax method. Our method requires that the NWs be properly configured on the platform, i.e. the NW cannot have any segments lying in the epipolar plane, to ensure that the complete shape is properly represented. Error analysis indicated that a large difference in tilt angles for the stereo image pairs can reduce representation errors. The 3D representation of the NWs was shown to be an important procedure to correctly measure the mechanical properties of these nanostructures. This work will be further developed for use in robotic nanomanipulation.

Supplementary information

The following information is available at: http://www.blackwellpublishing.com/products/journals/suppmat/JMI/JMI1418/JMI1418sm.htm

Appendix S1. Compressed source code.

MATLAB6.5.1 is required to run this program. The digitizing part (TUBE TRACER) was developed by Y. Fridman at the University of North Carolina, Chapel Hill (see Fridman *et al.*, 2003).

Acknowledgements

Funding for this work has been provided by a NASA/MSFC Phase II SBIR, contract no. NAS8-02102, through a subcontract from Lytec, LLC., by the National Science Foundation (NIRT program, grant no. 0304506, Dr Ken P. Chong, Program Director), and from the NASA University Research, Engineering and Technology Institute on Bio Inspired Materials (BIMat) under award no. NCC-1–02037 (Jeff Jordan, Program Manager). SEM was carried out at the Electron Probe Instrumentation Center of Northwestern University. We appreciate the comments by F. Fisher, K. M. Kohlhaas, and E. Zimney; we thank L. R. O. Hein for providing NIH Image Macro Tools and valuable advice.

References

Bishop, R.E.D. & Johnson, D.C. (1960) *Mechanics of Vibration.* Cambridge University Press, Cambridge.

Boyde, A. (1973) Quantitative photogrammetric analysis and qualitative stereoscopic analysis of SEM images. *J. Microsc.* **98**, 452–471.

Bullitt, E., Liu, A. & Pizer, S.M. (1997) Three-dimensional reconstruction of curves from pairs of projection views in the presence of error. I. Algorithms. *Med. Phys.* **24**, 1671–1678.

Chen, X., Zhang, S., Wagner, C.J., Ding, W. & Ruoff, R.S. (2004) Mechanical resonance of quartz microfibers and boundary condition effects. *J. Appl. Phys.* **95**, 4823–4828.

Cheng, Y., Hartemink, C.A., Hartwig, J.H. & Dewey, C.F. (2000) Three-dimensional reconstruction of the actin cytoskeleton from stereo images. *J. Biomech.* **33**, 105–113.

Dikin, D.A., Chen, X., Ding, W., Wagner, G. & Ruoff, R.S. (2003) Resonance vibration of amorphous SiO_2 nanowires driven by mechanical or electrical field excitation. *J. Appl. Phys.* **93**, 226–230.

Fridman, Y., Pizer, S.M., Aylward, S. & Bullitt, E. (2003) Segmenting 3D branching tubular structures using cores. *MICCAI 2003, Proceedings*, pp. 570–577.

Hartley, R. & Zisserman, A. (2000) *Multiple View Geometry in Computer Vision*, p. 607. Cambridge University Press, Cambridge.

Hein, L.R.O. (2001) Quantitative fractography by digital image processing: NIH Image macro tools for stereo pair analysis and 3-D reconstruction. *J. Microsc.* **204**, 17–28.

Hein, L.R.O., Silva, F.A., Nazar, A.M.M. & Amann, J.J. (1999) Three-dimensional reconstruction of fracture surfaces: area-matching algorithms for automatic parallax measurements. *Scanning*, **21**, 253–263.

Henri, C.J. & Peter, T.M. (1996) Three-dimensional reconstruction of vascular trees: theory and methodology. *Med. Phys.* **23**, 197–204.

Poncharal, P., Wang, Z.L., Ugarte, D. & de Heer, W.A. (1999) Electrostatic deflections and electromechanical resonances of carbon nanotubes. *Science*, **283**, 1513–1516.

Theron, A., Zussman, E. & Yarin, A.L. (2001) Electrostatic field-assisted alignment of electrospun nanofibers. *Nanotechnology*, **12**, 384–390.

Thong, J.T.L. & Breton, B.C. (1992) A topography measurement instrument based on the scanning electron microscope. *Rev. Sci. Instrum.* **63**, 131–138.

Timoshenko, S. (1936) *Theory of Elastic Stability*. McGraw–Hill, New York.

Treacy, M.M.J., Ebbesen, T.W. & Gibson, J.M. (1996) Exceptionally high Young's modulus observed for individual carbon nanotubes. *Nature*, **381**, 678–680.

Yu, M.-F., Wagner, G.J., Ruoff, R.S. & Dyer, M.J. (2002) Realization of parametric resonances in a nanowire mechanical system with nanomanipulation inside a scanning electron microscope. *Phys. Rev. B*, **66**, 073406-1–073406-4.